Available online at www.sciencedirect.com
ScienceDirect
Icarus 191 (2007) 486–496
ICARUS
www.elsevier.com/locate/icarus

The lunar exosphere: The sputtering contribution

P. Wurz [a,*], U. Rohner [a,1], J.A. Whitby [a], C. Kolb [b], H. Lammer [b], P. Dobnikar [c], J.A. Martín-Fernández [d]

[a] *Physikalisches Institut, Universität Bern, Sidlerstrasse 5, CH-3012 Bern, Switzerland*
[b] *Space Research Institute, Austrian Academy of Sciences, Schmiedlstrasse 6, A-8042 Graz, Austria*
[c] *Institute for Physics, University of Graz, Universitätsplatz 5/II, A-8010 Graz, Austria*
[d] *Department for Computer Science and Applied Mathematics, University of Girona, Edifici, P-IV, Campus Montilivi, E-17071 Girona, Spain*

Received 12 February 2007; revised 26 April 2007

Available online 24 May 2007

Abstract

We have extended our Monte Carlo model of exospheres [Wurz, P., Lammer, H., 2003. Icarus 164 (1), 1–13] by treating the ion-induced sputtering process from a known surface in a self-consistent way. The comparison of the calculated exospheric densities with experimental data, which are mostly upper limits, shows that all of our calculated densities are within the measurement limits. The total calculated exospheric density at the lunar surface of about 1×10^7 m^{-3} as result of solar wind sputtering we find is much less than the experimental total exospheric density of about 10^{12} m^{-3}. We conclude that sputtering contributes only a small fraction of the total exosphere, at least close to the surface. Because of the considerably larger scale height of atoms released via sputtering into the exosphere, sputtered atoms start to dominate the exosphere at altitudes exceeding a few 1000 km, with the exception of some light and abundant species released thermally, e.g. H_2, He, CH_4, and OH. Furthermore, for more refractory species such as calcium, our model indicates that sputtering may well be the dominant mechanism responsible for the lunar atmospheric inventory, but observational data does not yet allow firm conclusions to be drawn.

Keywords: Moon; Moon, surface; Atmospheres, composition

1. Introduction

Rather surprisingly, the composition and structure of the tenuous lunar atmosphere, actually an exosphere, remain poorly understood almost forty years after the first Apollo landings, and as recently as 1997 it has been suggested that we cannot account for 90% of the night-time exosphere (Stern et al., 1997, and references therein). The reasons for this are the difficulty of observations due to the very low number densities, and the complexity of models due to the multiplicity of mechanisms responsible for the input and loss of atomic species to and from the exosphere. These mechanisms include ion sputtering, photon stimulated desorption (PSD) and micro-meteoroid impact vaporization resulting in inputs to the atmosphere, and photoionization, surface adsorption and thermal escape resulting in losses from the lunar gravity field (e.g., Stern, 1999; Killen and Ip, 1999; Hunten and Sprague, 1997; Mendillo et al., 1999).

Within the last twenty years, much work has focused on the neutral sodium and potassium components of the exosphere as these can now be studied from the Earth (Potter and Morgan, 1988, 1998; Flynn and Mendillo, 1993), but the behavior of these elements may not be representative of other species as these are the elements probably most influenced by meteoritic influx and photon-induced desorption (Sprague et al., 1992). The composition of noble gases in the lunar atmosphere (largely inferred from studies of gas trapped in lunar regolith samples) indicates that these may be dominated by a solar wind source, but with additional contributions probably from the interior of the Moon (e.g., Hodges and Hoffman, 1975; Wieler et al., 1996). The latter idea is supported by observations of episodic outgassing of radon (Gorenstein et al., 1974a, 1974b; Hodges, 1975; see Lawson et al., 2005, for a review of the liter-

* Corresponding author. Fax: +41 31 631 44 05.
E-mail address: peter.wurz@space.unibe.ch (P. Wurz).
[1] Present address: Lawrence Livermore National Laboratory, Physics and Advanced Technologies Directorate, Livermore, CA 94551, USA.

0019-1035/$ – see front matter
doi:10.1016/j.icarus.2007.04.034

Table 1
Observational upper limits for lunar neutral elemental exosphere dayside number densities (ignoring hydrogen and noble gases) after Stern (1999)

Species	Detection method	Number density (cm^{-3})	Reference
O	Apollo 17 UV spectroscopy (1304 Å)	<500 (3σ)	Feldman and Morrison (1991)
N	Apollo 17 UV spectroscopy (1200 Å)	<600 (3σ)	Feastie et al. (1973)
C	Apollo 17 UV spectroscopy (1657 Å)	<200 (3σ)	Feldman and Morrison (1991)
S	Apollo 17 UV spectroscopy (1474 Å)	<150 (3σ)	Feldman and Morrison (1991)
Na	Ground-based spectroscopy (5889 Å)	35,70	Potter and Morgan (1988, 1998)
Si	Ground-based spectroscopy (3906 Å)	<48 (5σ)	Flynn and Stern (1996)
Al	Ground-based spectroscopy (3962 Å)	<55 (5σ)	Flynn and Stern (1996)
Ca	Ground-based spectroscopy (4227 Å)	<1 (5σ)	Flynn and Stern (1996)
K	Ground-based spectroscopy (7699 Å)	17	Potter and Morgan (1988)
Fe	Ground-based spectroscopy (3859 Å)	<380 (5σ)	Flynn and Stern (1996)
Ti	Ground-based spectroscopy (5036 Å)	<1 (5σ)	Flynn and Stern (1996)
Ba	Ground-based spectroscopy (5536 Å)	<0.2 (5σ)	Flynn and Stern (1996)
Al	HST UV spectroscopy	<11,000 (5σ)	Stern et al. (1997)
Mg	HST UV spectroscopy	<6000 (5σ)	Stern et al. (1997)

Note. Data from Apollo 17 are derived from averages of different observation positions.

ature). Because the solar wind impinges on the lunar surface H and He atoms are neutralized and are subsequently released to become part of the exosphere (e.g., Hinton and Taeusch, 1964; Johnson, 1971; Hodges, 1973, 1980). In contrast, the flux of heavier more refractory elements to the lunar atmosphere may be dominated by ion sputtering. In this case, the lunar surface material will be the primary source reservoir for elements in the lunar exosphere such as Si, Ti, Al, Fe, Mg, Ca, and O, which have not yet been observed directly. Table 1 shows upper limits for the abundances of these and some other elements. The exosphere densities at the surface of Na and K given in Table 1 are not only the result of sputtering but also to a larger extent most likely the result of photon stimulated desorption (PSD). In addition it has been estimated that up to 15% of the observed Na in the exosphere can be attributed to the impact of micro-meteors (Flynn and Mendillo, 1993).

Hodges (1973, 1980) modeled global distributions of H and He concentrations in the lunar exosphere and got results for He that are in good agreement with the Apollo 17 lunar surface mass spectrometer measurements. While in view of the absence of hydrogen the author proposed a model where the amounts are assumed to be below the measurement threshold and the majority of the hydrogen, which is of solar origin, is efficiently lost from the Moon by thermal and nonthermal escape processes. In the present work we investigate the contribution to the lunar neutral exosphere of heavy refractory elements released by ion sputtering.

A quantitative understanding of the processes that give rise to the lunar exosphere in a self consistent way will improve the general understanding of the exospheres of atmosphere-less bodies. For airless bodies the exosphere is directly connected to the planetary surface. Lunar exosphere measurements with the SARA instrument on the Indian Chandrayaan-1 mission, scheduled for launch in early 2008, will allow the testing of our model calculations (Bhardwaj et al., 2005). An important future application of models of exospheres of airless bodies will be the Hermean exosphere where measurements of its composition and structure will be performed by several instruments, to gain information not only about the exosphere itself but also about the surface composition of Mercury (Milillo et al., 2005). Our approach is to test our models against constraints obtained by current and future measurements of the lunar exosphere, and then to extend the models to the slightly different conditions relevant on Mercury. Although our modeling approach is quite general, we will concentrate on the predictions made for species where sputtering is expected to dominate the production rate. We do this first because it will allow a better check of the model (when good enough observational constraints are available), and secondly because the abundance of several of these species (e.g., Ca, Fe) is critical to constraining models for the formation and subsequent evolution of the Moon and especially Mercury.

2. Lunar surface composition

The topmost layer of the lunar surface consists largely of regolith, an unconsolidated "soil" layer of several meters thickness, made of lithic fragments, agglutinate grains and dust, continuously reworked and turned over by meteorite bombardment over geologic timescales (e.g., Chapter 7 in Heiken et al., 1991). This bombardment results in the introduction of some meteoritic material of less than 2 wt% in soils (Papike et al., 1998) and some local mixing of the surface. Laul and Papike (1980) were able to explain the composition of soil samples using between three and six end-members for each Apollo site, although the choice of end-members was adjusted for each site. In this work we have used measured regolith compositions reported by Papike et al. (1982) for the Apollo and Luna soil samples. These can be divided into the following categories: Highland, Ti-rich Mare, Ti-poor Mare and Kreep. These names reflect the dominant petrological component in these soils deduced using the same component analysis as Laul et al. (1982) and are between them believed to be broadly representative of the lunar surface. To simplify model calculations we simply averaged the values in each category (see Table 2), effectively giving a four-component model for the composition of lunar soils. Although the composition of the finest soil fractions differs from the bulk, we have assumed that the average bulk composition is repre-

Table 2
Lunar reference suite soils (including Apollo 15 sample 15601) for Highland, Kreep, low-Ti and high-Ti Mare regions

Reference suite	Size fraction	Si	Ti	Al	Fe	Mg	Ca	Na	K	Mn	Cr	O	Total
Highland soils													
64501,122	Bulk	16.26	0.10	11.72	1.26	2.62	6.61	0.31	0.05	0.02	0.03	61.03	100
67461,74	Bulk	16.09	0.08	12.31	1.26	2.08	6.74	0.30	0.03	0.02	0.02	61.09	100
22001,35	>125 μm	∗16.18	0.13	9.95	2.18	5.19	5.43	0.24	0.03	0.03	0.05	60.59	100
72501,15	Bulk	16.57	0.39	8.69	2.91	5.47	4.91	0.31	0.08	0.04	0.07	60.57	100
Average		16.31	0.17	10.66	1.90	3.84	5.92	0.29	0.05	0.03	0.04	60.82	100
Kreep soils													
12001,599	Bulk	17.21	0.79	5.51	5.38	5.80	4.37	0.35	0.12	0.07	0.12	60.29	100
12033,464	Bulk	17.47	0.64	6.23	4.80	5.11	4.43	0.48	0.19	0.06	0.11	60.47	100
14163,778	Bulk	17.37	0.44	7.70	3.22	5.26	4.49	0.50	0.26	0.04	0.06	60.66	100
Average		17.35	0.62	6.48	4.47	5.39	4.43	0.44	0.19	0.06	0.10	60.47	100
Low-Ti Mare soils													
12001,599	Bulk	17.21	0.79	5.51	5.38	5.80	4.37	0.35	0.12	0.07	0.12	60.29	100
15601	Bulk	17.39	0.57	4.64	6.39	6.27	4.09	0.22	0.05	0.08	0.17	60.12	100
21000,5	Bulk	∗16.80	0.98	6.82	5.15	4.51	4.72	0.27	0.05	0.07	0.09	60.54	100
24999,6	Bulk	∗17.29	0.29	5.29	6.48	5.55	4.56	0.20	0.01	0.09	0.14	60.09	100
Average		17.30	0.66	5.56	5.85	5.53	4.44	0.26	0.06	0.08	0.13	60.26	100
High-Ti Mare soils													
10084,1591	Bulk	15.85	2.16	6.19	5.07	4.58	5.14	0.30	0.07	0.07	0.09	60.48	100
A17 drill core, Unit E	1000–20 μm	15.51	2.49	5.17	5.60	6.03	4.41	0.30	0.04	0.07	0.13	60.24	100
A17 drill core, Unit D	1000–20 μm	15.65	2.44	4.92	5.91	5.82	4.47	0.31	0.04	0.08	0.13	60.22	100
A17 drill core, Unit C	1000–20 μm	15.92	1.63	6.00	5.09	6.01	4.60	0.30	0.05	0.06	0.12	60.22	100
A17 drill core, Unit B	1000–20 μm	16.21	1.60	6.03	4.91	5.87	4.46	0.32	0.07	0.06	0.12	60.34	100
A17 drill core, Unit A	1000–20 μm	16.01	1.72	5.87	5.15	5.90	4.52	0.31	0.05	0.07	0.12	60.28	100
Average		15.86	2.01	5.70	5.29	5.70	4.60	0.31	0.05	0.07	0.12	60.30	100

Note. Data were taken from Papike et al. (1982) and are reported in mol%. Original literature on Luna soil chemistry lacks in reporting values for Si (Laul and Papike, 1981). Therefore, we assigned average wt% values of Si to empty Luna Si entries (marked by asterisk). All data are normalized to 100%.

sentative of the surface. This assumption may be inaccurate if the finest fraction occupies a large fraction of the surface area because the sputtering mechanism is only effective in the uppermost 100 nm of a solid.

3. The sputter model

In the present model we only consider particle sputtering by the impact of energetic ions, which in the case of the Moon is the solar wind, on the planetary surface in a self-consistent way. Particle sputtering will release all species from the surface into space reproducing more or less the local surface composition on an atomic level. Preferential sputtering of the different elements of a compound will lead to a surface enrichment of those elements with low sputtering yields in the top-most atomic layers. However, the steady-state composition of the flux of sputtered atoms will reflect the average bulk composition. Thus, particle sputtering, when operative, will give us compositional information about the refractory elements of the bulk surface.

The energy distribution for particles sputtered from a solid, $f(E_e)$, with the energy E_e of the sputtered particle, has been given as (Sigmund, 1969)

$$f(E_e) = \frac{6E_b}{3-8\sqrt{E_b/E_c}} \frac{E_e}{(E_e+E_b)^3} \left\{1 - \sqrt{\frac{E_e+E_b}{E_c}}\right\}, \qquad (1)$$

where E_b is the surface binding energy of the sputtered particle and E_c is the cut-off energy. The cut-off energy E_c, which is the maximum energy that can be imparted to a sputtered particle by a projectile particle with energy E_i, is given by the limit imposed by a binary collision between a projectile atom M_1 and the target atom M_2 (to be sputtered) as

$$E_c = E_i \frac{4M_1M_2}{(M_1+M_2)^2}. \qquad (2)$$

Fig. 1 shows examples of the energy distribution for typical atoms sputtered from the lunar surface under solar wind bombardment. Note that the maximum of the energy distribution (Eq. (1)) is at $E_{\max} = E_b/2$, with E_b ranging from fractions of an eV to several eV depending on species and matrix. At higher energies the distribution falls off with E_e^{-2}, which is also observed experimentally (e.g., Thompson et al., 1968; Husinsky et al., 1985). Note that if the energy of the incident ion is so low that the cut-off energy E_c approaches the binding energy the energy distribution of sputtered atoms becomes rather narrow. Moreover, ion sputtering operates above an energy threshold of about 30 eV, which is exceeded significantly by the solar wind ions.

The polar angle distribution of sputtered atoms, $f(\alpha)$, for polycrystalline surfaces is best described by a quadratic angular dependence, $f(\alpha) \propto \cos^2\alpha$ for laboratory experiments (Hofer, 1991). However, Cassidy and Johnson (2005), found

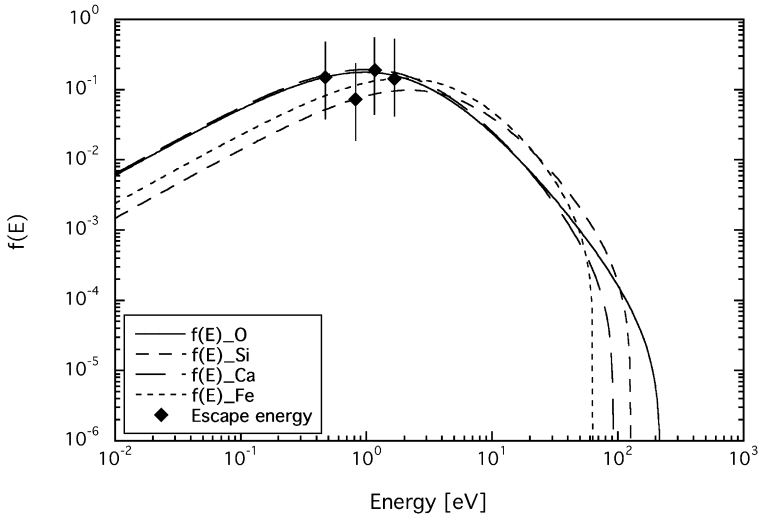

Fig. 1. Energy distribution for sputtered O, Si, Ca, and Fe atoms according to Eq. (1) using incident protons of 1 keV energy. The symbols indicate the escape energy for these atoms, the vertical bars are only for better visibility.

recently that for the fine-grained and porous regolith a better choice is $f(\alpha) = \cos\alpha$, which is used in our calculations. For the azimuth angle we used a uniform distribution over 2π. Having the energy, the azimuth and elevation angle we can calculate all three components of the initial particle velocity $\mathbf{v}$ and the trajectory of each sputtered particle. Using many such trajectories the vertical density profile $N_i(h)$ can be calculated using our Monte Carlo code (Wurz and Lammer, 2003). Either the exospheric density at the surface or the column density can be used for comparison with observational data.

The flux Φ_i of particles sputtered from the planetary surface can be calculated as

$$\Phi_i = \Phi_{\rm ion} Y_i^{\rm tot} = \Phi_{\rm ion} Y_i^{\rm rel} C_i, \tag{3}$$

where $\Phi_{\rm ion}$ is the ion flux onto the surface and $Y_i^{\rm tot}$ the total sputter yield of species i from the surface, i.e., the elemental mixture discussed above. The total sputter yield can be broken up into a relative sputter yield $Y_i^{\rm rel}$ and C_i the atomic abundance of species i on the surface. The total sputter flux of species i is also given by

$$\Phi_i = N_i(0)\langle v_i\rangle \tag{4}$$

with $N_i(0)$ the exospheric particle density at the surface ($h = 0$), and $\langle v_i\rangle$ the average velocity of sputtered particles. Combining Eqs. (3) and (4) we calculate the exospheric density at the surface for species i as

$$N_i(0) = \Phi_{\rm ion} Y_i^{\rm tot} \frac{1}{\langle v_i\rangle}. \tag{5}$$

In the Monte Carlo calculation $N_i(0)$ is used as a starting point to calculate the density profile from the sputtering process for a given surface composition. We can easily integrate the exospheric density profile to obtain the column density, which is the typical measurement obtained from telescopic observations of the exosphere.

The average release velocity is derived from the sputter distribution (see Eq. (1) and Fig. 1) as

$$\begin{aligned}\langle v_i\rangle &= \frac{\int v f(v)\,{\rm d}v}{\int f(v)\,{\rm d}v} \\ &= \frac{1}{2} v_1^2 v_2 \left(-\frac{3v_1^2 + 5v_2^2}{(v_1^2 + v_2^2)^2} + \frac{3\arctan(v_2/v_1)}{v_1 v_2} \right)\end{aligned} \tag{6}$$

with the abbreviations

$$v_1 = \sqrt{\frac{2E_{b,i}}{m_2}} \quad \text{and} \quad v_2 = \frac{4v_{\rm SW}}{M_1 + M_2},$$

where $E_{b,i}$ is the binding energy of species i in the particular chemical mix of the surface, m_2 is the mass of the sputtered atom in kg, and M_1 and M_2 are the atomic numbers for the incoming and the sputtered atom, respectively. Note that the most probable velocity is $v_{\rm mp} = \sqrt{E_{b,i}/m_2}$, which is lower than the average release speed by a factor of about 3.3. These velocities have to be compared to the lunar escape speed of 2.376 km s^{-1}. If we take oxygen as an example, with a binding energy of $E_b =$ 2.0 eV, we get $\langle v_i\rangle = 11.57$ km s^{-1} and $v_{\rm mp} = 3.47$ km s^{-1}, which both exceed the escape velocity considerably. The same is true for the other elements and is illustrated in Fig. 1. Thus most of sputtered atoms escape the lunar gravity field.

In conclusion, if we know the flux of ions impinging on the planetary surface, $\Phi_{\rm ion}$, then with the sputter yields $Y_i^{\rm tot}$ we can calculate the sputtered flux, the surface density, the density profile, and the column density ab initio and compare these numbers with the observations using our Monte Carlo code (Wurz and Lammer, 2003). The addition of sputter yields together with a surface composition is the most significant improvement to the exosphere model reported earlier (Wurz and Lammer, 2003). Such calculations for the Moon will be shown in the next chapter.

The heavy ions in the solar wind are highly charged because of the million-degree hot solar corona. Oxygen, for example, is present in the solar wind with charges states of typically +6

and +7, iron with charge states in the range from +8 to +12. These high charge states mean that these ions have high internal energies, e.g. 295 eV for O^{6+} and 1055 eV for Fe^{10+}, which have to be compared to their kinetic energies in the solar wind of typically 16 keV for oxygen and 56 keV for iron. It has been argued that the sputter yield for highly charged ions impacting on a planetary surface is increased by a factor of 10 to 1000 as a result of their high internal energy (Shemansky, 2003). The laboratory data on sputter yields for highly charged ions have been reviewed by Aumayr and Winter (2004), and we will briefly summarize their findings here. For metallic surfaces and semiconductors (Si and GaAs) no deviation of the sputter yield for highly charged ions from the sputter yield of singly charged ions was found, with the highest charge states investigated being Ar^{9+} and Xe^{25+}. Moreover, all the measured sputter yields agree with the TRIM calculations, a software package which considers only the kinetic energy of the impacting ion (Ziegler and Biersack, 1985; Ziegler, 2004). For ionic crystals (NaCl and LiF) a pronounced increase with ionic charge state was observed; for NaCl the sputter yield increased by a factor of 4 for Ar^{8+} ions compared to Ar^{+} ions, for LiF the sputter yield increased by a factor of 25 for Ar^{14+} ions compared to Ar^{+} ions. Note that Ar charge states in the solar wind range from +8 to +11. For oxides, which are the best analogue for the lunar surface, a clear signature of a sputter yield increase for highly charged ions was observed for SiO_2 and Al_2O_3. For SiO_2 this increase was about 3 for Ar^{8+} ions compared to Ar^{+} ions, and about 65 for Xe^{25+} ions compared to Ar^{+} ions. Similar enhancements were found for the Al_2O_3 surface. However, this enhancement is strongly dependent upon the ion dose the surface has been exposed to. After a removal of about a monolayer from the oxide surface, the sputter yield for highly charged ions drops to about the values for singly charged ions. Removal of a monolayer of surface material corresponds to a heavy ion flux of a few 10^{13} ions cm^{-2} at solar wind energies, which takes about two months at Earth orbit. This reduction in sputter yield is attributed to the top-most surface layers becoming reasonably conductive (by preferential loss of oxygen and the creation of crystal defects) and thus the highly charged ions become decharged, i.e., they lose their internal energy, when they approach the surface. In conclusion, we do not consider an enhancement of the sputter yield by highly charged solar wind ions in this paper.

4. Solar wind sputter yields for lunar soil material

We calculated the total sputter yield, Y_i^{tot}, for all species i for the four reference surface compositions discussed above using the TRIM.SP software (Biersack and Eckstein, 1984; Ziegler, 2004). The TRIM.SP software has been optimized to and usually reproduces sputter yields very well (e.g., Gillen et al., 2002; Aumayr and Winter, 2004). Also the energy distribution of sputtered particles is reproduced well by TRIM.SP, even the high energy tails (e.g., Gillen et al., 2002). In the sputter process the energy of the impacting particle is distributed among atoms at and near the surface in the form of a collision cascade, which leads to the release of some of these atoms from the surface. The flux of sputtered atoms is considered to be proportional to the abundance of that element on the surface (see Eq. (3)), which is used widely in laboratories for surface composition analysis. Nevertheless, we calculated the individual sputter yields for all elements for the four reference surfaces to avoid making this assumption.

Depending on the abundance of a species in the lunar surface between 75,000 and 1,700,000 projectile ions were simulated with TRIM.SP to assure good statistics. As projectile ions we used a mixture of protons and alpha particles, 95 and 5%, respectively. Heavy solar wind ions are not considered here since their total abundances is about 0.1% in the solar wind (Wurz, 2005, and references therein). The solar wind velocities we investigated are in the range from 300 to 800 km s^{-1} to cover the typical variation of solar wind conditions. The sputter yields obtained from the TRIM.SP calculation for the four reference surface compositions are shown in Fig. 2. We calculated different angles of incidence of the ions on the surface since the sputter yield increases with shallower impact. The sputter yield is a strong function of the incident angle of the ion with the maximum of the sputter yield being between 55° and 85° (with respect to the surface normal) depending and the mass of the incident and the target atom (Sigmund, 1969, 1981). However, this is only true for smooth surfaces. As soon as the surface is rough (for example because of prolonged ion bombardment) the angle of incidence dependence is gone and the sputter yield has about the same value as for a smooth surface at 45° impact (Küster et al., 2000). Since lunar regolith certainly can be regarded as a rough surface we used the sputter yields for 45° in the following calculations.

For solar wind speeds other than the calculated ones, we numerically interpolate between the calculated values. Since the velocity dependence of the sputter yields has a simple form, this interpolation is straightforward and no significant uncertainty is expected from this procedure.

The sputter yields presented in Fig. 2 are the yields for solid grains. The porosity of the surface is not included at this stage, but later in the calculation. As one can see from Fig. 2 the sputter yields are low, around 0.1 surface atom per solar wind ion. The reason for the low sputter yields is that the solar wind is mostly composed of protons; the 5% alpha particles typically contribute 30% to the total sputter yield. Oxygen or iron ions of the solar wind contribute at most 1% to the sputter yield, other heavy ions even less. The velocity dependence is such that the maximum of the sputter yield typically results from solar wind speeds in the range between 300 and 500 km s^{-1}.

5. Exospheric densities from sputtering

Using the previously mentioned sputter yields and the energy and angular distributions for the sputtering process, we calculated exospheric density profiles for the four categories of lunar surface compositions. When calculating the sputter release for a space-weathered planetary surface one also has to account for the porosity of the surface (Cassidy and Johnson, 2005). For lunar regolith breccias a typical porosity of $25 \pm 7\%$ was found (Warren, 2001, and references therein). However,

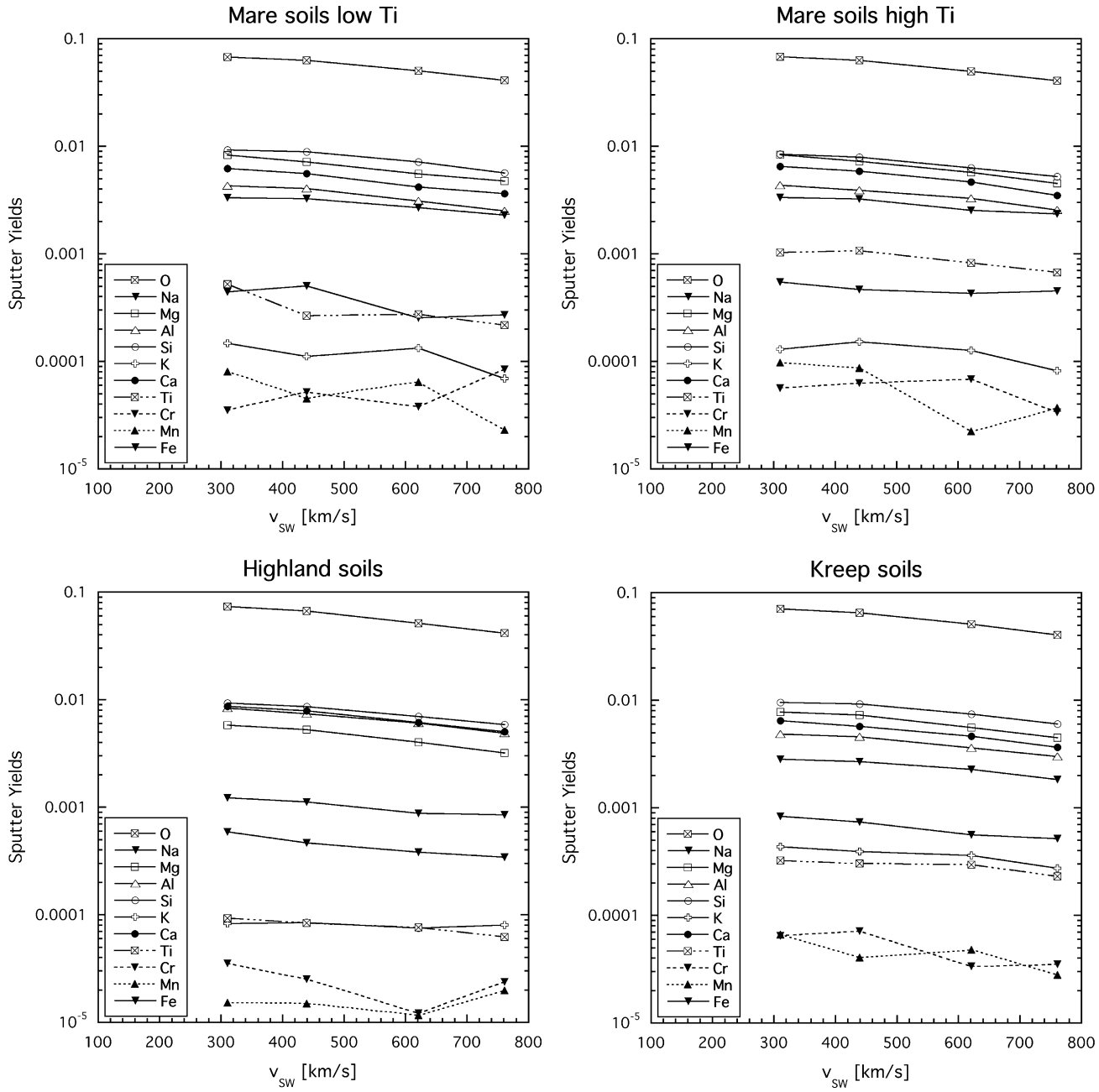

Fig. 2. Sputter yields (i.e., sputtered atoms per incoming ion) for solar wind ions for the four compositional types of the lunar surface.

since sputtering probes the topmost surface it is more appropriate to use the porosity from cores, which is between 46 and 57% (Costes et al., 1970). Note that porosity values up to 80% have been reported (Kaula, 1968). In our calculations we use a porosity of 50%, which seems to be a good compromise for a global characterization of the porosity of the uppermost lunar surface.

We studied three solar wind cases of solar wind speed and flux: (1) $v_{SW} = 450\ \mathrm{km\,s^{-1}}$, $f_p = 2.0 \times 10^{12}\ \mathrm{m^{-2}\,s^{-1}}$, (2) $v_{SW} = 530\ \mathrm{km\,s^{-1}}$, $f_p = 2.65 \times 10^{12}\ \mathrm{m^{-2}\,s^{-1}}$, and (3) $v_{SW} = 670\ \mathrm{km\,s^{-1}}$, $f_p = 2.68 \times 10^{12}\ \mathrm{m^{-2}\,s^{-1}}$, since these solar wind parameters prevailed during the measurement campaigns used to determine the upper limits given in Table 1 (based on the OMNI data base). The calculations were performed for the sub-solar point, for other points the sputter yields, and thus the exosphere densities, will scale with the cosine of the zenith angle. The results of these calculations are shown in Fig. 3. Note that the sputtering process releases surface atoms (and molecules) with high energies with respect to the lunar gravitational field (see Eq. (1)). Practically all sputtered atoms escape from the Moon.

In almost all cases the values predicted by our model are consistent with the observational upper bounds shown in Table 1. The one exception is for the abundance of calcium atoms, which is about the same and sometimes exceeding the 5-sigma upper bound of 1 atom per $\mathrm{cm^3}$ of the measurement, in particular for the highland soils. However, it should be borne in mind that the upper bound is derived from a spatially integrated measurement and is not appropriate for a pure highland soil, and

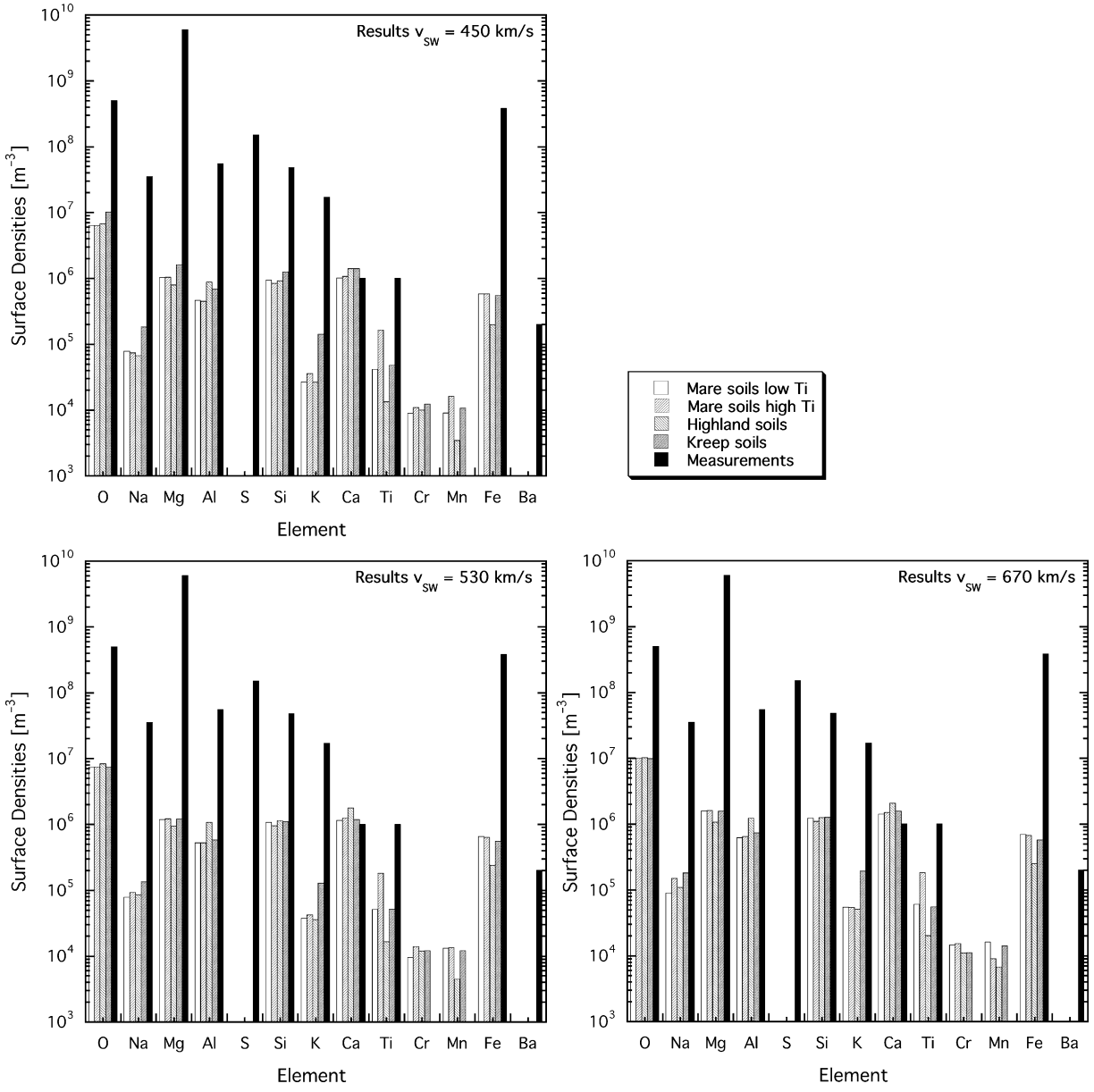

Fig. 3. Comparison of the calculations of the lunar exospheric surface densities at the sub-solar point with measurements (from Table 1). Note that the experimental data are upper limits.

also that this is an unusually high solar wind speed. Moreover, the calculated density is for the sub-solar point. If one assumes a cosine law for the sputter yield because of the reduction of ion flux with lower zenith angle, the integrated density value for the sun-lit surface is a factor of 2π smaller and thus well inside with the experimental upper bound. This apparent disagreement of the model with the observational bounds is therefore insignificant. Clearly better observational data are needed in order to test the assumptions and parameters of the model and this will probably require in situ measurements.

Overall, the calculated exospheric densities for solar wind sputtering are low, and the sum of all calculated elements gives a surface density of about 1×10^7 m^{-3}. The total density of all measured species is variable, but amounts to about 10^{12} m^{-3} on the dayside (Stern, 1999). Most of these species are volatiles being released thermally or via PSD from the lunar surface and thus have a low scale height in the atmosphere. This result is in agreement with the observations of the lunar exosphere during a lunar eclipse where the Moon was inside the Earth magnetosphere and sputtering by energetic ions should be a negligible contribution to the lunar exosphere. But no variations in exospheric column contents at least for observable species like Na were observed (Mendillo et al., 1999), and the authors concluded that solar wind sputtering may not be the main surface release process which is in agreement with our results. However, in a later study a hysteresis effect in the sodium density was observed, whereby the sodium density was lower coming out of the magnetotail than it was coming in, which was interpreted that the solar wind causes a mobilization of the sodium on the lunar surface (Potter et al., 2000).

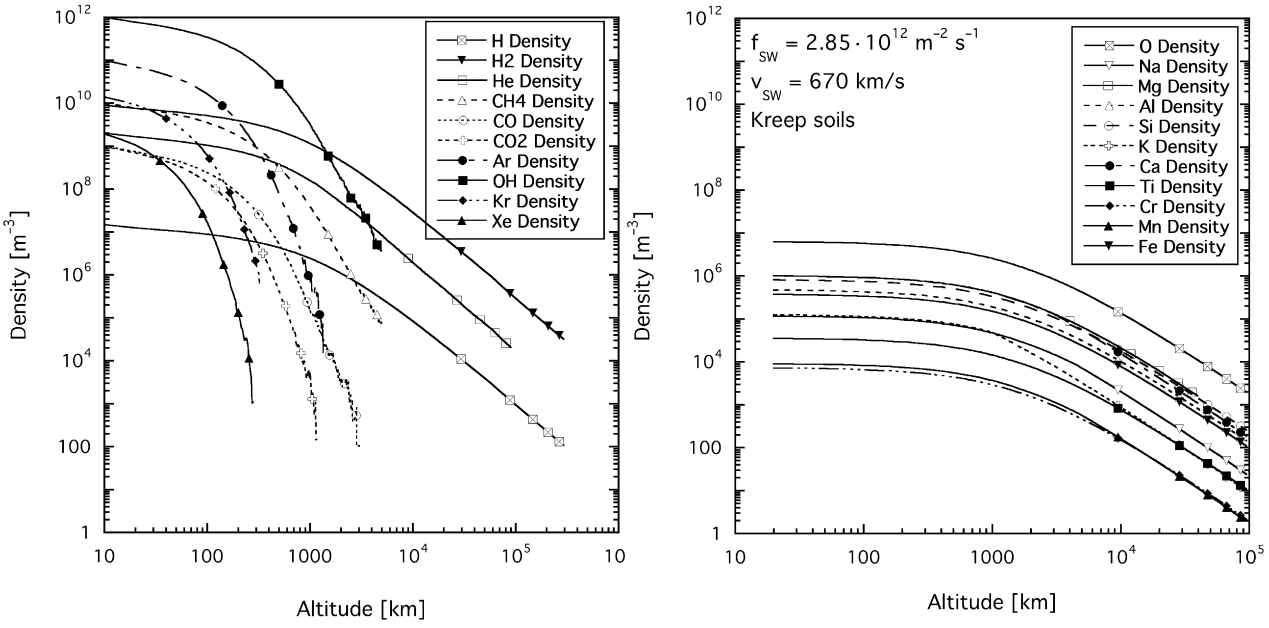

Fig. 4. Left: density profiles of thermally released atoms and molecules based on the exospheric surface densities from Stern (1999). Right: density profiles of sputtered atoms from Kreep soils for $v_{SW} = 670\ \mathrm{km\,s^{-1}}$ and $f_p = 2.85 \times 10^{12}\ \mathrm{m^{-2}\,s^{-1}}$. Both calculations are done for the sub-solar point.

Sputtered atoms have more energy than thermally released species and thus a larger scale height. Fig. 4 shows the density profiles for sputtered atoms in comparison with thermally released species, in both cases for the sub-solar point. To model the thermal release we assumed a surface temperature at the sub-solar of 400 K and used our Monte Carlo code to calculate the density profiles (Wurz and Lammer, 2003). For the thermally released species we used the surface densities for the known species compiled by Stern (1999) as input for our calculation of the density profiles. Clearly, the volatiles dominate the exosphere close to the lunar surface by several orders of magnitude. Because of the much larger scale height of atoms released via sputtering into the exosphere, they start to dominate the exosphere at altitudes exceeding at a few 1000 km, with the exception of some light and abundant species released thermally, H, H_2, and He. Because of their large densities CH_4 and OH may also reach high altitudes. Note that the surface density reported for OH is only an upper limit (Stern, 1999). Moreover, these heavier hydrogen compounds could be ionized by the solar radiation and particle environment and picked up by the solar wind (Hodges, 1973).

One can see from our studies that the exospheric densities are very low, and thus it will be an experimental challenge to measure these densities accurately, especially from an orbiting spacecraft. For the sputtered particles one can also hope for transient events in the solar wind, i.e., coronal mass ejections (CMEs), during which the solar wind flux can increase by one to two orders of magnitude in intensity and so will the exospheric densities. The duration of a CME is typically a day at Earth orbit. In any case, sputtering, together with micro-meteorite impact vaporisation, are the only means to bring refractory elements into the exosphere.

6. Solar wind induced composition changes on the surface

Since the Moon is unprotected from the solar wind by a magnetic field the total Sun-facing surface is constantly bombarded by solar wind ions except when the Moon is inside the Earth's magnetotail. The total flux of solar wind ions onto the Moon's surface is typically $4.5 \times 10^{12}\ \mathrm{ions\,m^{-2}\,s^{-1}}$, which is variable with time. This ion flux corresponds to $8.5 \times 10^{-15}\ \mathrm{kg\,m^{-2}\,s^{-1}}$. Integrated over the lunar surface we get a total of $4.3 \times 10^{25}\ \mathrm{ions\,s^{-1}}$, which corresponds to $0.081\ \mathrm{kg\,s^{-1}}$. When considering such a high influx of solar material we have to worry if the composition of the topmost surface of the Moon may reflect the solar composition because of deposition (implantation) of solar material. Fortunately, protons and alpha particles make up more than 99% of the solar wind ions, and the lunar surface is saturated with hydrogen and helium. The heavy ions (from carbon to iron and up) together are about 0.1% of the solar wind ions in the number flux (Wurz, 2005, and references therein). Although the sputter yield of solar wind ions is rather low (about to 0.07 atoms/ion considering the mix of solar wind ions and the porosity) it is more than sufficient to remove all implanted heavy ions. For heavy atoms (from carbon to iron and up), the removal via sputtering exceeds the input from solar wind by 1 to 3 orders of magnitude, because the abundance of heavy ions in the solar wind is very low. Since the gravitational field of the Moon is low, practically all sputtered atoms escape because their typical ejection speed exceeds the lunar escape speed of $2376\ \mathrm{m\,s^{-1}}$.

The meteoritic infall on the Moon is estimated to be $5.202 \times 10^{-16}\ \mathrm{kg\,m^{-2}\,s^{-1}}$ (Bruno et al., 2006), which corresponds to $0.0197\ \mathrm{kg\,s^{-1}}$ or $5.68 \times 10^{23}\ \mathrm{atoms\,s^{-1}}$ for the full lunar surface. Meteoritic infall values of $6.3 \times 10^{-16}\ \mathrm{kg\,m^{-2}\,s^{-1}}$ and a range of $(4.8–6.3) \times 10^{-16}\ \mathrm{kg\,m^{-2}\,s^{-1}}$ the have been reported

earlier by Gault et al. (1972) and by Zook (1975), respectively. The mass flux of meteoritic infall is low in comparison to the solar wind. Moreover, for meteorite infall the typical energy per atom is much lower (typical impact velocities of 30 km s^{-1}) than for solar wind. Thus, we conclude that on average the release of particles into the exosphere via meteorite infall is less important than by solar wind induced sputtering aside from episodic events associated with the known meteoroid showers. Interestingly, Zook (1975) estimated that the meteoritic fraction in the released particles by an impact is about 20%.

In addition to loss of sputtering atoms from the exosphere, ionization of exospheric species plays an additional role as an escape process from the Moon. On the other hand it is expected that $\leqslant$40% of the ionized exospheric particles may collide with the surface (Manka and Michel, 1970) where they may also act as sputter agents of the surface material or where they can be implanted in the surface. Such a process is considered as an explanation of the ^{40}Ar that is found in lunar soil samples (Manka and Michel, 1970; Hodges, 1975). Whether an ion will be implanted in deeper surface layers of the lunar soil, or will be adsorbed at the top surface layer or is released again, depending on the impact energy (Bühler et al., 1966; Manka and Michel, 1970). From sputter experiments with Ar ions it is known that about 60% of the higher energy fraction of the back-scattered ions with energies $1 < E_{\mathrm{Ar}} \leqslant 3$ keV may be implanted in the surface at depths where they can not be ejected by sputtering again.

For Ar ions with energies $\geqslant$3 keV almost 100% will be trapped in the lunar grains (Bühler et al., 1966; Manka and Michel, 1970). Manka and Michel (1970) found that depending on the IMF field strength, between 5–8% of the released exospheric ^{40}Ar will be implanted in the surface material due to ionization and subsequent interaction and acceleration by the $\mathbf{v} \times \mathbf{B}$ force in the solar wind. A detailed study that will investigate the role of heavy exospheric ions to surface sputtering is beyond the scope of this work but is considered for the future. Generally, we expect that there is no large alteration of the lunar surface composition because of the implantation of solar material. However, this will be different for heavier planetary bodies without atmosphere, for example Mercury.

Hapke et al. (1975) conducted sputtering experiments on artificial glass, whose chemical composition was similar to Apollo 11 rocks, with the proton beam orientation at 45° from the surface normal to simulate space weathering by ion bombardment. The forward sputtered atoms were captured by a Mo foil substrate. The enrichment ratio (film/parent), measured by means of electron microprobe analysis, gave clear evidence for recondensation with increasing atomic weight of atoms on the foil substrate, especially dominated by deposition of the element Fe. Hapke et al. (1975) and Hapke (2001, and references therein) ascribe this phenomenon to be a key process in the course of maturation and spectral reddening of surface soils upon space weathering. Alkali elements were detected in the film at very low levels indicating strong depletion in relation to the parent, but no quantitative data were reported in Hapke et al. (1975). However, since practically all sputtered atoms escape the lunar gravitation field we conclude that selective recondensation of atoms is not a relevant process for changing the surface composition.

7. Conclusions

In almost all cases the values predicted by our model are consistent with the observational upper bounds shown in Table 1. The only exception is the abundance of calcium atoms for which the calculated density is commensurate with the 5-sigma upper bound of 1 atom per cm^3 as we discussed above. The sum of all calculated elements released by the sputtering process gives a surface density of about 1×10^7 m^{-3} depending on solar wind parameters and surface composition. The total density of all measured species is variable, but amounts to about 10^{12} m^{-3} on the dayside (Stern et al., 1997; Stern, 1999). We conclude that at the surface the exosphere is dominated by elements released via thermal processes and PSD. Since both the solar wind and the solar illumination follow the same zenith angle dependence (neglecting the small aberration of the solar wind because of the motion of the Earth around the Sun) this conclusion is true for the entire dayside of the Moon. Micro-meteorite impact vaporisation is considered to contribute to the exosphere even less than sputtering but will be important on the night side of the Moon because of the absence of the other processes. At higher altitudes the sputtered contribution becomes more significant and eventually dominates, because of the low scale height of thermally released particles.

Given the long range of released species on ballistic trajectories, both thermally released as well as sputtered species, small-scale fluctuations in the surface composition will be smeared out with increasing altitudes. As a first-order approximation, the radius of the footprint of an in situ measurement performed at a certain altitude will be the same as the altitude. For the Chandrayaan-1 mission orbiting at 100 km above the surface only coarse compositional maps of the lunar surface can be expected. However, we do expect to observe changes in the exospheric composition reflecting the varying surface.

We also conclude that the influx of solar wind and sputtering will not cause a change in the elemental composition of the surface (other than the saturation of the surface with H and He) because more heavy atoms are sputtered from the surface than are delivered by the solar wind. Since most of the sputtered atoms escape, selective recondensation cannot operate. However, the thermally released particles do not escape, with the exception of H (63% escape), H_2 (47% escape), and He (28% escape), and are far more abundant near the surface. Their redistribution (day–night) and processing by UV light may cause a change in the chemical composition of the surface.

Acknowledgments

The OMNI data were obtained from the GSFC/SPDF OMNIWeb interface at http://omniweb.gsfc.nasa.gov. The financial support of the Swiss National Science Foundation is gratefully acknowledged. P. Dobnikar, C. Kolb, H. Lammer and J.A. Martín-Fernández acknowledge support from the "Büro

für Akademische Kooperation und Mobilität" of the Austrian Academic Exchange Service under the ÖAD-Acciones Integradas project 2006/2007. The chemical variability at planetary surfaces—implications for exogenic processes.

References

Aumayr, F., Winter, H., 2004. Potential sputtering. Philos. Trans. R. Soc. London A 362, 77–102.

Bhardwaj, A., Barabash, S., Futaana, Y., Kazama, Y., Asamura, K., Sridharan, R., Holmström, M., Wurz, P., Lundin, R., 2005. Low energy neutral atom imaging on the Moon with the SARA Instrument aboard Chandrayaan-1 mission. J. Earth Syst. Sci. 114 (6), 749–760.

Biersack, J.P., Eckstein, W., 1984. Sputtering of solids with the Monte Carlo program TRIM.SP. Appl. Phys. A 34, 73–94.

Bruno, M., Cremonese, G., Marchi, S., 2006. Neutral sodium atoms release from the surface of the Moon induced by meteoroid impacts. Mon. Not. R. Astron. Soc. 367, 1067–1071.

Bühler, F., Geiss, J., Meister, J., Eberhardt, P., Huneke, J.C., Signer, P., 1966. Trapping of the solar wind in solids—I. Earth Planet. Sci. Lett. 1, 249–255.

Cassidy, W., Johnson, R.E., 2005. Monte Carlo model of sputtering and other ejection processes within a regolith. Icarus 176, 499–507.

Costes, N.C., Carrier, W.D., Mitchell, J.K., Scott, R.F., 1970. Apollo 11 soil mechanics investigation. Science 167, 739–741.

Feastie, W.G., Feldman, P.D., Henry, R.C., Moos, H.W., Barth, C.A., Thomas, G.E., Donahue, T.M., 1973. A search for far-ultraviolet emission from the lunar atmosphere. Science 182 (11), 710–711.

Feldman, P.D., Morrison, D., 1991. The Apollo 17 ultraviolet spectrometer: Lunar atmosphere measurements revisited. Geophys. Res. Lett. 18 (11), 2105–2109.

Flynn, B., Mendillo, M., 1993. A picture of the Moon's atmosphere. Science 261, 184–186.

Flynn, B.C., Stern, S.A., 1996. A spectroscopic survey of metallic species abundances in the lunar atmosphere. Icarus 124, 530–536.

Gault, D.E., Hörz, F., Hartung, J.B., 1972. Effects of microcratering on the lunar surface. Proc. Lunar Sci. Conf. 3, 2713–2734.

Gillen, D.R., Graham, W.G., Goelich, A., 2002. Sputtering of copper atoms by keV atomic and molecular ions: A comparison of experiment with analytical and computer based models. Nucl. Instrum. Methods B 194, 409–416.

Gorenstein, P., Golub, L., Bjorkholm, P., 1974a. Detection of radon at the edges of lunar maria with the Apollo alpha-particle spectrometer. Science 183, 411–413.

Gorenstein, P., Golub, L., Bjorkholm, P., 1974b. Radon emanations from the Moon, spatial and temporal variability. Earth Moon Planets 9, 129.

Hapke, B., 2001. Space weathering from Mercury to the asteroid belt. J. Geophys. Res. 106 (E5), 10039–10074.

Hapke, B., Cassidy, W., Wells, E., 1975. Effects of vapor-phase deposition processes on the optical, chemical, and magnetic properties of the lunar regolith. Moon 13, 339–353.

Heiken, G.H., Vaniman, D.T., French, B.M., 1991. Lunar Sourcebook: A User's Guide to the Moon. Cambridge Univ. Press, Cambridge, England, p. 736.

Hinton, F.L., Taeusch, D.R., 1964. Variation of the lunar atmosphere with the strength of the solar wind. J. Geophys. Res. 69, 1341–1347.

Hodges Jr., R.R., 1973. Helium and hydrogen in the lunar atmosphere. J. Geophys. Res. 78, 8055–8064.

Hodges Jr., R.R., 1975. Formation of the lunar atmosphere. Moon 14, 139–157.

Hodges Jr., R.R., 1980. Methods for Monte Carlo simulation of the exospheres of the Moon and Mercury. J. Geophys. Res. 85, 164–170.

Hodges Jr., R.R., Hoffman, J.H., 1975. Implications of atmospheric ^{40}Ar escape on the interior structure of the Moon. Proc. Lunar Sci. Conf. 6, 3039–3047.

Hofer, W.O., 1991. Angular, energy, and mass distribution of sputtered particles. In: Behrisch, R., Wittmaack, K. (Eds.), Sputtering by Particle Bombardment. Springer, Berlin, pp. 15–90.

Hunten, D.M., Sprague, A.L., 1997. Origin and character of the lunar and mercurian atmospheres. Adv. Space Res. 19 (10), 1551–1560.

Husinsky, W., Girgis, I., Betz, G., 1985. Doppler shift laser fluorescence spectroscopy of sputtered and evaporated atoms under Ar^+ bombardment. J. Vac. Sci. Technol. B 3 (5), 1543–1545.

Johnson, F.S., 1971. Lunar atmosphere. Rev. Geophys. Space Phys. 9, 813–823.

Kaula, W.M., 1968. An Introduction into Planetary Physics: The Terrestrial Planets. Wiley, New York, p. 331.

Killen, R.M., Ip, W.-H., 1999. The surface-bounded atmospheres of Mercury and the Moon. Rev. Geophys. 37 (3), 361–406.

Küster, M., Eckstein, W., Dose, V., Roth, J., 2000. The influence of surface roughness on the angular dependence of the sputter yield. Nucl. Instrum. Methods B 145, 320–331.

Laul, J.C., Papike, J.J., 1980. The lunar regolith: Comparative chemistry of the Apollo sites. Proc. Lunar Sci. Conf. 11, 1307–1340.

Laul, J.C., Papike, J.J., 1981. Comparative chemistry of size fractions from the Apollo and Luna sites. Meteoritics 16, 347.

Laul, J.C., Papike, J.J., Simon, S.B., 1982. The Apollo 14 regolith—Chemistry of cores 14210/14211 and 14220 and soils 14141, 14148, and 14149. Proc. Lunar Sci. Conf. 13, A247–A259.

Lawson, S.L., Feldman, W.C., Lawrence, D.J., Moore, K.R., Elphic, R.C., Belian, R.D., 2005. Recent outgassing from the lunar surface: The Lunar Prospector alpha particle spectrometer. J. Geophys. Res. 110, doi:10.1029/2005JE002433.

Manka, R.H., Michel, F.C., 1970. Lunar atmosphere as a source of Argon-40 and other lunar surface elements. Science 169, 278–280.

Mendillo, M., Baumgardner, J., Wilson, J., 1999. Observational test for the solar wind sputtering origin of the Moon's extended sodium atmosphere. Icarus 137, 13–23.

Milillo, A., Wurz, P., Orsini, S., Delcourt, D., Kallio, E., Killen, R.M., Lammer, H., Massetti, S., Mura, A., Barabash, S., Cremonese, G., Daglis, I.A., DeAngelis, E., Di Lellis, A.M., Livi, S., Mangano, V., Torkar, K., 2005. Surface–exosphere–magnetosphere system of Mercury. Space Sci. Rev. 117, 397–443.

Papike, J.J., Simon, S.B., Laul, J.C., 1982. The lunar regolith—Chemistry, mineralogy, and petrology. Rev. Geophys. Space Phys. 20, 761–826.

Papike, J.J., Ryder, G., Shearer, C.K., 1998. Lunar samples. Rev. Mineral. 36 (5), 1–234.

Potter, A.E., Morgan, T.H., 1988. Discovery of sodium and potassium vapor in the atmosphere of the Moon. Science 241, 675–680.

Potter, A.E., Morgan, T.H., 1998. Coronagraphic observations of the lunar sodium exosphere near the lunar surface. J. Geophys. Res. 103 (E4), 8581–8586.

Potter, A.E., Killen, R.M., Morgan, T.H., 2000. Variation of lunar sodium during passage of the Moon through the Earth's magnetotail. J. Geophys. Res. 105, 15073–15084.

Shemansky, D.E., 2003. The role of solar wind heavy ions in the space environment. AIP Conf. Proc. 663, 687–696.

Sigmund, P., 1969. Theory of sputtering. I. Sputtering yield of amorphous and polycrystalline targets. Phys. Rev. 184, 383–416.

Sigmund, P., 1981. Sputtering by ion bombardment: Theoretical concepts. In: Behrisch, R. (Ed.), Sputtering by Ion Bombardment, vol. I. Springer, Berlin, pp. 9–71.

Sprague, A.L., Kozlowski, R.W., Hunten, D.M., Grosse, F.A., 1992. The sodium and potassium atmosphere of the Moon and its interaction with the surface. Icarus 96, 27–42.

Stern, S.A., 1999. The lunar atmosphere: History, status, current problems, and context. Rev. Geophys. 37 (4), 453–491.

Stern, S.A., Parker, J.W., Morgan, T.H., Flynn, B.C., Hunten, D.M., Sprague, A.L., Mendillo, M., Festou, M.C., 1997. An HST search for magnesium in the lunar atmosphere. Icarus 127, 523–526.

Thompson, M.W., Farmery, B.W., Newson, P.A., 1968. A mechanical spectrometer for analyzing the energy distribution of sputtered atoms of copper and gold. Philos. Mag. 18 (152), 361–383.

Warren, P.H., 2001. Porosities of lunar meteorites: Strength, porosity and petrologic screening during the meteorite delivery process. J. Geophys. Res. 106 (E5), 10101–10111.

Wieler, R., Kehm, K., Meshik, A.P., Hohenberg, C.M., 1996. Secular changes in the xenon and krypton abundances in the solar wind recorded in single lunar grains. Nature 382, 46–49.

Wurz, P., 2005. Solar wind composition. In: The Dynamic Sun: Challenges for Theory and Observations, ESA SP-600, vol. 5.2. Noordwijk, The Netherlands, pp. 1–9.

Wurz, P., Lammer, H., 2003. Monte-Carlo simulation of Mercury's exosphere. Icarus 164 (1), 1–13.

Ziegler, J.F., 2004. SRIM-2003. Nucl. Instrum. Methods B 219, 1027–1036.

Ziegler, J.F., Biersack, J.P., 1985. The Stopping Power and Ranges of Ions in Matter. Pergamon, New York. http://www.srim.org/.

Zook, H.A., 1975. The state of meteoritic material on the Moon. Proc. Lunar Sci. Conf. 6, 1653–1672.